Compression of glycolide-h4 to 6GPa

Compression of glycolide-h4 to 6 GPa

Authors

Ian B. Hutchison[a], Craig L. Bull[b]*, Willliam G. Marshall[b], Simon Parsons[c], Andrew J. Urquhart[d] and Iain D.H. Oswald[a]*

[a]Strathclyde Institute of Pharmacy and Biomedical Sciences, University of Strathclyde, 161 Cathedral Street, Glasgow, G4 0RE, UK

[b]ISIS Neutron and Muon Source, Science and Technology Facilities Council, Rutherford Appleton Laboratory, Harwell, Didcot, OX11 0QX, UK

[c]School of Chemistry and Centre for Science at Extreme Conditions, The University of Edinburgh, Kings Buildings West Mains Road, Edinburgh, EH9 3JJ, United Kingdom

[d]Department of Micro- and Nanotechnology, Technical University of Denmark, Ørsteds Plads, Building 345Ø, Lyngby, 2800 Kgs., Denmark

Correspondence email: craig.bull@stfc.ac.uk; iain.oswald@strath.ac.uk

Synopsis   Fully hydrogenated glycolide ($C_4H_4O_4$) has been studied as a function of pressure on the High Pressure beamline, PEARL, at ISIS Neutron and Muon Source. It undergoes a phase transition but remains monomeric to 6 GPa.

Abstract   This study details the structural characterisation of glycolide-h4 as a function of pressure to 6 GPa using neutron powder diffraction on the PEARL instrument at ISIS Neutron and Muon source. Glycolide-h4, rather than its deuterated isotopologue, was used in this study due to the difficulty of deuteration. The low-background afforded by Zirconia-Toughened Alumina (ZTA) anvils nevertheless enabled the collection of data suitable for structural analysis to be obtained to a pressure of 5 GPa. Glycolide-h4 undergoes a reconstructive phase transition at 0.15 GPa to a previously identified, form-II, which is stable to 6 GPa.

1. Introduction

The study of molecular materials at high pressure has been a fruitful area for structural science with many compounds showing significant structural changes at elevated pressures.(Zakharov, Seryotkin, *et al.*, 2016, Zakharov, Goryainov, *et al.*, 2016, Hobday *et al.*, 2016, Fabbiani *et al.*, 2007, Zakharov & Boldyreva, 2014, Moggach *et al.*, 2008, Wood *et al.*, 2008) High-pressure crystallographic techniques have been used to identify new polymorphs and solvates which are unknown under ambient conditions.(Moggach *et al.*, 2008, Olejniczak *et al.*, 2016, Oswald & Pulham, 2008, Oswald *et al.*, 2008) In particular, we have been investigating the phenomenon of solid-state pressure-induced

polymerisation and the role polymorphism has on the reaction product.(Johnston *et al.*, 2014, Marshall *et al.*, 2015, Oswald & Urquhart, 2011) There have been a number of spectroscopic studies (Murli & Song, 2010, Bini *et al.*, 2012, Ceppatelli *et al.*, 2000, Chelazzi *et al.*, 2005, Ciabini *et al.*, 2002, Ciabini *et al.*, 2007, Santoro *et al.*, 2003, Aoki *et al.*, 1989, Kojima *et al.*, 1995, Murli *et al.*, 2012) but only a few diffraction-based studies (Jin *et al.*, 2013, Wilhelm *et al.*, 2008) that have investigated chemical reactions in a range of aromatic, olefinic materials. Recent work of Sun et al (Sun *et al.*, 2017) has highlighted the role of neutron powder diffraction and solid-state NMR to elucidate the pathways to various products from the compression of acetylene depending on the pressure achieved. Ring systems have been investigated using spectroscopy and observed to undergo chemical reactions, e.g. carosine (Murli *et al.*, 2012) and L,L-lactide (Ceppatelli *et al.*, 2011). In the solid-state, L,L-lactide is stable up to 17 GPa which was the highest pressure achieved in the study but under high pressure and temperature conditions begins to polymerise.

Glycolide ($C_4H_4O_4$; Figure 1) is the pre-cursor to poly(glycolic acid) and undergoes a ring-opening polymerisation to the polymeric product under ambient pressure (Dechy-Cabaret *et al.*, 2004). We previously investigated glycolide at high pressure, revealing the formation of a new high-pressure polymorph (form-II) between 0.4 and 0.58 GPa which was unusual in being recoverable at ambient pressure and accessible on a gram scale when prepared using a large volume press (Hutchison *et al.*, 2015). The transition to form-II is reconstructive and the molecule shows a significant conformational change to become disordered about an inversion centre. In this paper, we will discuss the changes in the crystal structure of glycolide from ambient pressure to 6 GPa using high-pressure neutron powder diffraction.
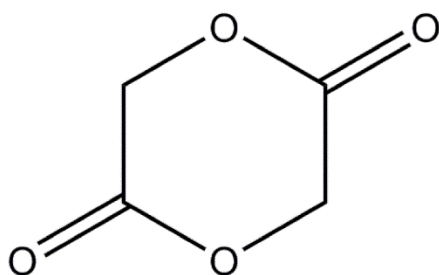
**Figure 1** Schematic of glycolide

2. Experimental

2.1. High-pressure neutron powder diffraction

High-pressure neutron powder diffraction data were collected using the PEARL diffractometer at the UK spallation neutron source, ISIS, located at the STFC Rutherford Appleton Laboratory.(Bull *et al.*,

2016) Glycolide-h_4 was purchased from Sigma-Aldrich and recrystallized from a saturated acetone solution before being ground at ambient temperature. An encapsulated titanium-zirconium gasket (Marshall & Francis, 2002) and one of the ZTA anvils were cooled to 263 K under a nitrogen purge before loading the gasket with glycolide, lead (for use as a pressure marker)(Schulte & Holzapfel, 1995, Vohra & Ruoff, 1990, Mao *et al.*, 1990) and a 1:1 mixture of pentane-d_{12} and isopentane-d_{12} as a pressure-transmitting medium (PTM) (Klotz *et al.*, 2009). Cooling the gasket and anvil was necessary because both components of the PTM are highly volatile; the nitrogen purge minimised condensation of atmospheric moisture onto the gasket/anvil assembly. The gasket/anvil assembly was quickly inserted into a Paris-Edinburgh V3 press before applying 6 tonnes of load to ensure the gasket was sealed but not applying significant pressure to the sample. The time-of-flight (TOF) neutron powder diffraction data were collected and reduced using procedures outlined in our previous work.(Johnston *et al.*, 2014) Data suitable for structure refinement were collected over a period of 8 hours in increments of ~1 GPa interspersed with shorter runs of 2-4 hours to allow monitoring of the of the unit cell parameters.

The data were analysed with TOPAS Academic software. (Coelho, 2012) The initial pattern, at approximately ambient pressure, was consistent with glycolide form-I (Figure 2). Patterns collected above 0.15 GPa indicated that the sample had transformed to form-II. Only the data for form-II was suitable for Rietveld refinement. For these refinements a model defined using a Z-matrix with all atoms set to 0.5 occupancy was used to account for atoms generated by the inversion symmetry. The use of the Z-matrix was a convenient way of describing the molecular geometry especially in the disordered form-II. The starting model for the high pressure structure refinements was taken from our previously-reported X-ray study.(Hutchison *et al.*, 2015) Torsional angles were allowed to refine and showed the puckered nature of the rings under pressure. The final refined unit cell parameters are listed in Table S1.

Figure 2 shows indicative patterns below and above the phase transition which shows a change in diffraction intensity between the two spectra. The intensity of the glycolide signal increased by ~25% over the course of the form-I-to-II transition, which suggests that the initial sample contained an amorphous component, which recrystallized into form-II on increasing the pressure.
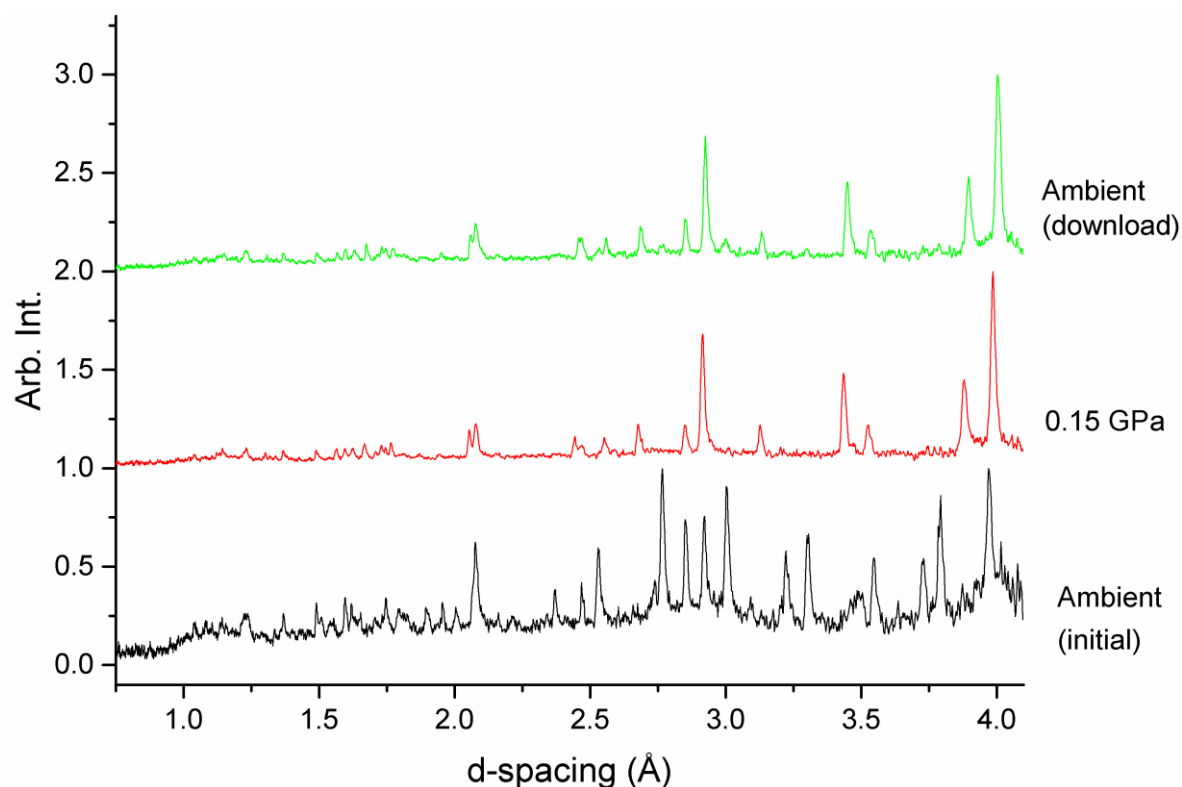
Figure 2 Normalised data for the compression of glycolide-h_4 at selected pressures: Ambient pressure (form-I); 0.15 GPa (form-II); and decompression to ambient pressure showing retention of form-II to ambient pressure which is in-line with our previous seeding experiment (Hutchison *et al.*, 2015). The drop-off in intensity due to the incoherent scattering of the hydrogen atoms can clearly be observed at approximately at ~1.0 Å. Fits of the data can be found in Figure S1.

2.2. PIXEL calculations

Form-II of glycolide is an orthorhombic structure with the molecule disordered over an inversion centre. PIXEL calculations were carried out on an ordered model in $P2_12_12_1$. Electron densities were calculated using Gaussian09 (Frisch *et al.*, 2009) with the MP2/6-31G** basis set. The PIXEL results were analysed using processPIXEL (Bond, 2014).

2.3. Other programs

Pucker was to analyse the conformational changes in the molecule as a function for pressure (Gould *et al.*, 1995). EosFit7.0Gui was used to determine the equation of state of form-II of glycolide. (Angel Ross *et al.*, 2014) Mercury CSD 2.0 was used to visualise the structures and in the production of the Figures.(Macrae *et al.*, 2008)

3. Results and Discussion

3.1. Effect of pressure on glycolide-h4

Form-I of glycolide crystallises in space group $P2_1/n$ with Z'=2. The molecules show conformations that are mixture of twist-boat and boat conformation (Table 1). PIXEL calculations indicate that the most important intermolecular interaction is between the carbonyl groups (-34.9 kJmol^{-1}).(Hutchison *et al.*, 2015)   These types of interaction have been extensively studied by Allen *et al*. (Allen *et al.*, 1998) and shown to be as competitive with hydrogen bonds. The structure possesses anti-parallel carbonyl interactions between the independent molecules (3.1111(16) Å, -34.9 kJmol^{-1}, Figure 3). The dimers of molecules then interact through a sheared parallel interaction (3.2141(16) Å, -14.7 kJmol^{-1}, Figure 3). Both of these interactions are somewhat shorter than the average values for these interactions from the database (3.33 and 3.45 Å for the anti-parallel and shear-parallel respectively). The C=O...C angles (107.50° & 61.28°) are at the high end of the distributions observed by Allen *et al. (Allen et al., 1998)* however their study showed that the shear motif tends to occur between molecules exhibiting pi-stacking. The lack of pi stacking in the present structures perhaps explains the deviation of the geometric parameters away from typical values. Allen *et al.* also computed the ideal interaction values for anti-parallel interactions using in propanone as a model compound. They used intermolecular perturbation theory with varying intermolecular distance and demonstrated that an ideal separation is 3.02 Å and angle of 90-91° (-22 kJmol^{-1}).
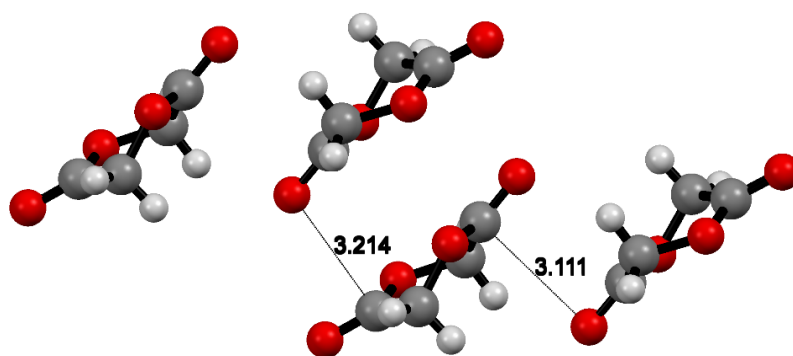
Figure 3 Crystal structure of form-I of glycolide showing the carbonyl anti-parallel interaction (3.1111(16) Å) and interaction between the dimers (3.2141(16) Å).

Our previous work in a diamond anvil cell demonstrated that on compression of form-I, a reconstructive phase transition occurs at 0.41 GPa to form-II (*Pbca*). We noted at the time that particle size is an important factor in the speed of transition i.e. a powdered sample underwent a polymorphic transition more rapidly than larger crystallites. From our neutron diffraction experiments, in this study, the phase transition to Form II was observed to occur by 0.15 GPa which is

lower than previously identified. The use of the powder in this experiment will have contributed to the lower transition pressure by reducing the kinetic barrier that the single crystal imposes allowing for a more accurate determination of the phase transformation pressure.

Form-II compresses monotonically up to a pressure of 5.89 GPa (Figure 4). Refinement of the unit cell parameters shows a decrease in the unit cell volume of 20% between 0.4 and 5.9 GPa. The bulk modulus determined for form-II of glycolide is 6.6(4) GPa with a V_0 of 461.9(8) $Å^3$, $K' =$ 14.0(7) using a 3rd-order Birch-Murnaghan Equation of State (Figure 4) which is in line with other organic materials lacking hydrogen bonding, e.g. Rubrene K= 8.2(8) GPa & K' = 9.4(9),(Bergantin *et al.*, 2014) anthracene K= 8.4(6) GPa & K' = 6.3(4),(Oehzelt *et al.*, 2006) and a little softer than extensively hydrogen-bonded organic solids e.g. L-alanine is K= 13.4(7) GPa and K' = 7.0(3).(Funnell *et al.*, 2011) The compression of the unit cell is anisotropic with the *a*-axis showing greatest compression (10%) followed by *b*- (7.3%), and *c*-axis (4.6%). Since the structure is orthorhombic, the principal axes of the strain tensor are aligned with the unit cell axes.
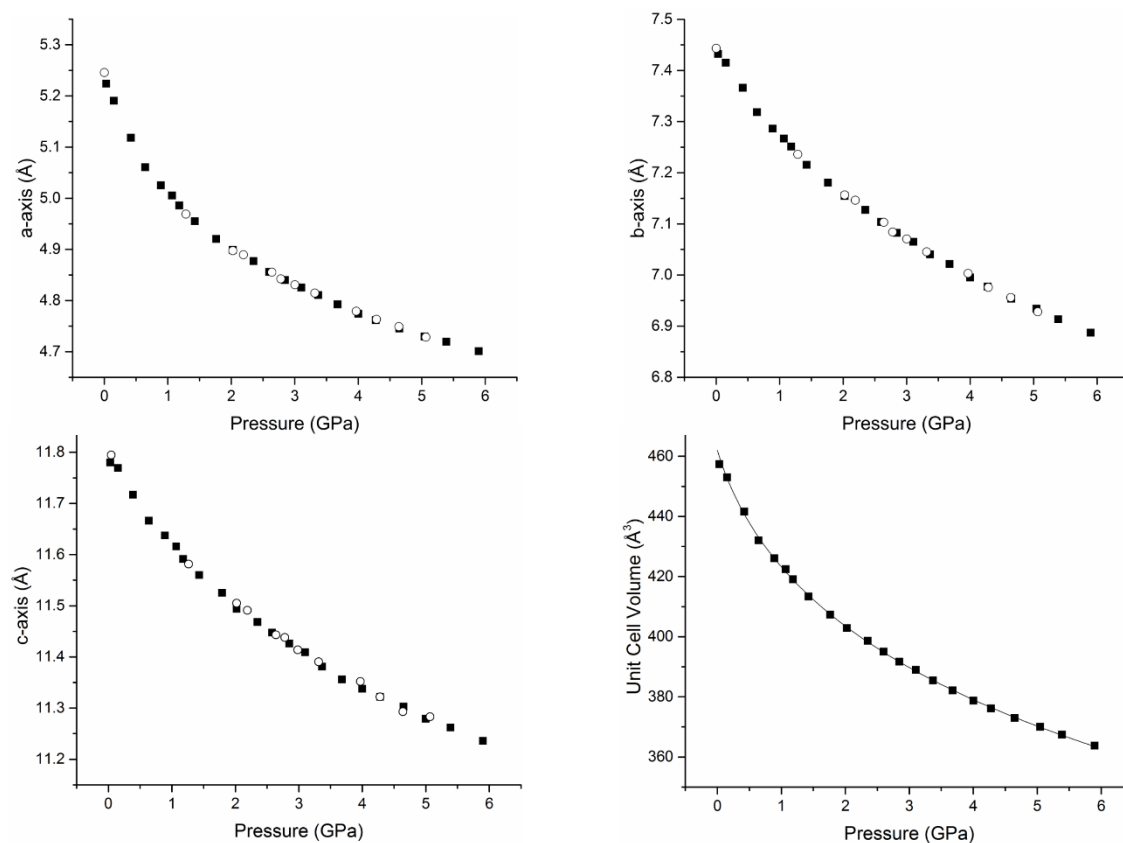
Figure 4 The compression of the unit cell parameters of form-I of glycolide. The black squares representing the compression and the hollow circles represent the parameters on decompression. No hysteresis is observed. The errors for the parameters are smaller than the symbols. Equation of State for form-II glycolide-h_4 (bottom right). The line represents the fit to the data using a 3rd-order Birch-Murnaghan Equation of State (V_0 of 461.9(8) $Å^3$, K = 6.6(4) GPa, K' = 14.0(7)). The pressure

variation of the individual unit cell parameters have been fitted. For the axial cell parameters, this analysis modelled the pressure variation of $ln(a)$, $ln(b)$ and $ln(c)$ by means of a low-order (typically quadratic) polynomials. Using this simple model, least squares fits of the form-II unit cell parameters yielded the following values for the initial compressibilities $\beta_a = 0.0468(20)$ GPa^{-1}, $\beta_b = 0.0247(7)$ GPa^{-1} and $\beta_c = 0.0162(5)$ GPa^{-1}, where $\beta_a = -(1/a)(\partial a/\partial p)$.

As in form-I, the molecules in form-II adopt a mixture of a twist-boat and boat conformation, but with a greater proportion of the latter (Table 1). As the pressure applied reaches 4 and 5 GPa the conformation tends towards the boat conformation which is energetically closer to the Form I conformations.

Table 1   Ring puckering analysis for glycolide under variable pressure. The analysis was performed using the program, *Pucker* (Gould *et al*., 1995) using the $P2_12_12_1$ description of the structure to allow for the input of one molecule with refined atomic positions description. Single point energy calculations were performed in Gaussian09 (Frisch *et al.*, 2009) with the MP2/6-31G** basis set.

	Percentage component			Relative conformational energy (kJmol^{-1})
	Chair	Twist-boat	Boat	
Form-I Mol. 1; 0 GPa	1	38	61	0
Form-I Mol. 2; 0 GPa	0	42	58	0.48651
Form-II; 0 GPa	16	51	33	36.10719
0.4 GPa	6	65	29	42.66359
1.8 GPa	12	71	17	16.98935
2.6 GPa	7	74	19	35.63827
4.0 GPa	8	49	43	20.43952
5.0 GPa	16	41	43	24.38591

Form-II is a layered structure with the layers extending over the *ab*-plane (Figure 5). Glycolide does not possess any hydrogen bond donating groups hence relies on CH…O, carbonyl and van der Waals interactions for stabilisation. Form-II does not possess the carbonyl interactions of form-I instead opting for a configuration whereby the molecules interact via a herring bone motif where the ether group is orientated towards the face of the neighbouring molecule (-23.4 kJmol^{-1}, current work). From the packing arrangement in Figure 5 the central molecule interacts its four nearest neighbours within the *ab*-layer (Figure 5a; red and black dotted lines) through interactions that

are largely coulombic (-21.5 & -19.5 kJmol^{-1}) and dispersive (-21.4 &-16.7 kJmol^{-1}; Interactions 1 & 2; Table S3). The use of PIXEL calculations allow us to map out the intermolecular potentials for all the close interactions in the crystal structure as distances are compressed. From these observations it can be noted that Interactions 1 and 2 lie at the bottom of this potential at an ideal distance at the lowest pressure of 0.4 GPa. These interactions becoming immediately less stabilising as they are compressed (Figure 6 & 7).
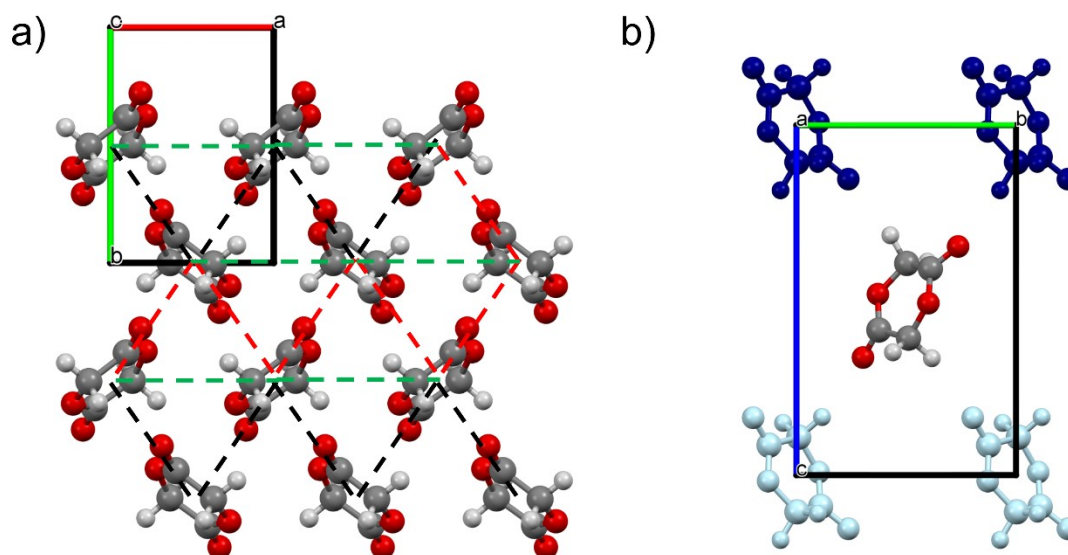

Figure 5 Form-II of glycolide viewed down a) the *c*-axis showing how the *ab* layers are arranged with the two strongest interactions indicated by red (Interaction 1) and black (Interaction 2) dotted lines and the third strongest by the green (Interaction 3) dotted lines ; b) the fourth (Interaction 4; dark blue) and fifth (Interaction 5; light blue) strongest interactions in form-II.

As noted from the compression of the cell parameters the *a*-axis is the most compressible direction which is parallel to Interaction 3 (green dotted line). The PIXEL calculations show that of the three most energetic interactions, this contact has the shallowest potential, and it is only above 2.5 GPa that the magnitude of the interaction energy begins to decrease. This suggests that by analysing the intermolecular potentials in this way, we may be able to understand which directions in the crystal structure are the most compressible. This would be particularly useful in lower symmetry crystals where the principal axes of strain tensor do not correspond to the cell directions.

Interactions 4 and 5 are formed between molecules in different layers and they interact in a slightly different way. (Figure 5a) The molecules involved in these interactions are aligned such that there is an almost linear interaction between C-H…OC (170°) *cf.* Interactions 1 and 2 where the molecules interact side-on. We believe that this has impact on the compression of the cell and the energies of the interactions. The *c*-axis is the least compressible despite the voids being concentrated between the *ab*-layers. As the nearest point of contact the linear nature of the C-H…OC interaction is likely to be providing resistance to the compression and will be the major contributor to the repulsion

term (Figure 7). At the same time there is an equal stabilisation effect as the molecules come closer together through lower coulombic, polarisation and dispersive energy contributions to the total energy of the interaction hence the energies of the interactions remain relatively constant over the compression.

Due to the limitations of the pressure capabilities of the pressure-transmitting media it was not possible to compress further however Raman data collected on a sample to 8.03 GPa show little change apart from a pressure shift (Figure S3). We monitored the sample at this pressure for 8 days but the spectra are not substantially different. The sample was compressed further to 10.4 GPa and it showed chemical stability of glycolide to this pressure. As a reference, l,l-lactide is stable to 17.3 GPa with no signs of polymerising.
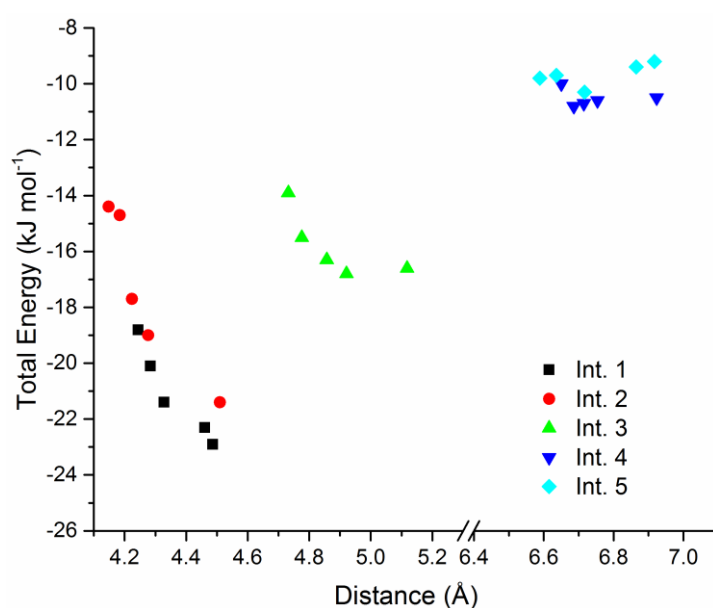
Figure 6 Interaction energies for the top five interactions in glycolide-h_4 form-II. Interactions 1-3 are observed between molecules in the *ab* layers.
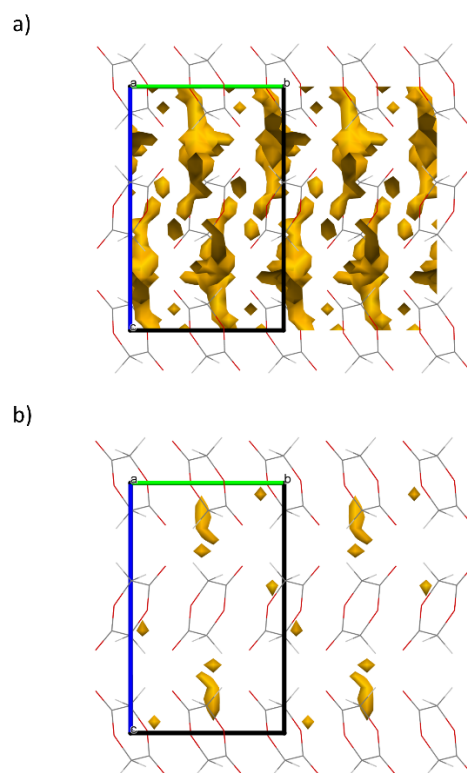
Figure 7 The void space in the crystal structures at a) 0.4 GPa and b) 5.0 GPa calculated from geometry optimised structure due to the disorder in the model. The probe radius was set to 0.2 Å and the grid spacing set to 0.5 Å giving a void volume of 5.3% of unit cell volume at 0.4 GPa and 0.4% at 5.0 GPa. Notably, the last void space remaining is that observed between the layers along the *c*-axis.

3.2. Decompression behaviour

Overall, from our diffraction experiment glycolide remains molecular in nature up to 6 GPa with evidence of stability to 10 GPa from Raman data (Figure S3). There is no evidence of any polymerisation occurring which was part of our hypothesis for looking at monomeric compounds under pressure. Our previous work on acrylic and methacrylic acid (Johnston *et al.*, 2014, Marshall *et al.*, 2015) demonstrated that polymerisation could occur on decompression but on release of pressure form-II persists to ambient pressure although due to the constraints of allocated beamtime the longevity of this form is unknown (Figures 2 & 8). From our previous work we observed that the crystals from a seeded solution of the high-pressure form lasted 12 days (Hutchison *et al.*, 2015).
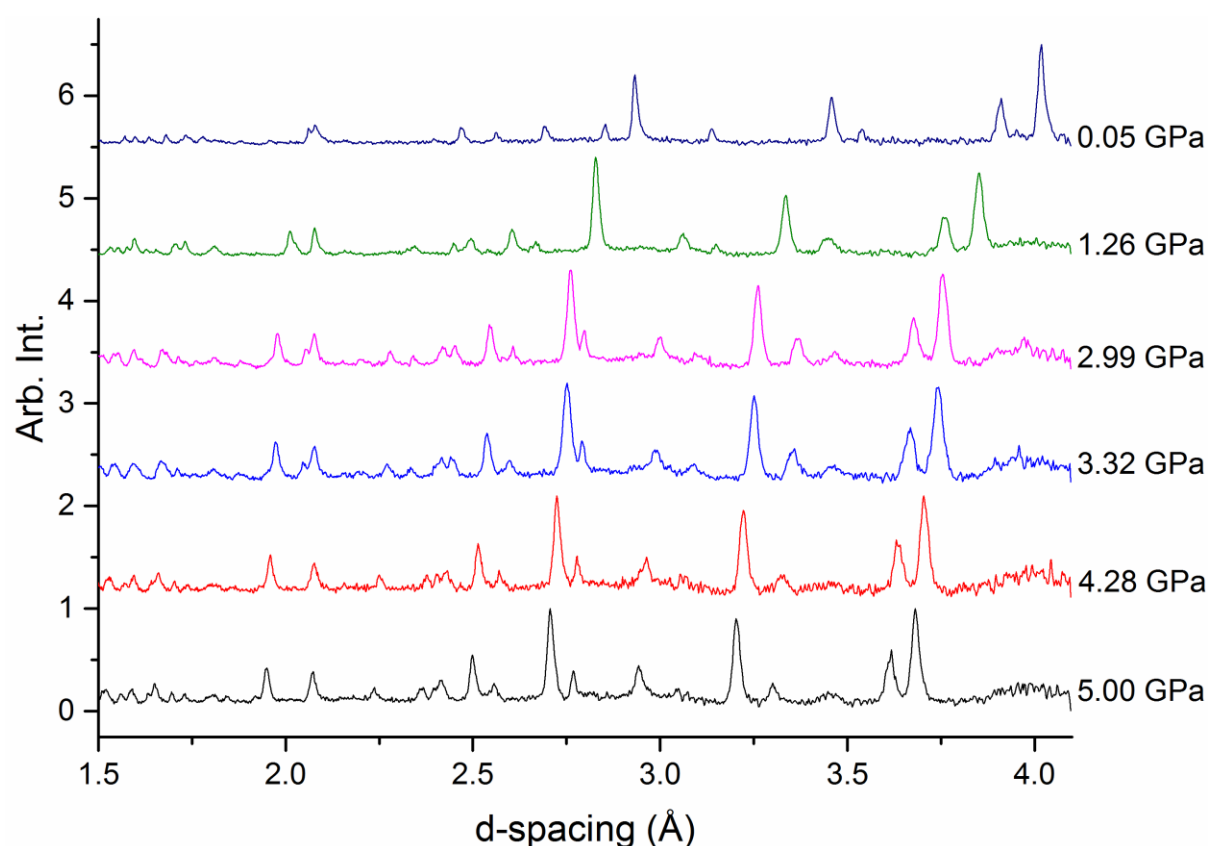
Figure 8 The decompression of glycolide from 5 GPa to ambient pressure showing the recovery of Form II.

3.3. Effect of hydrogenation on diffraction pattern

The disadvantage of investigating hydrogenous samples using neutron powder diffraction comes from the incoherent scattering of hydrogen which causes the powder diffraction pattern to have a higher and noisier background (Wilson *et al.*, 2014). In general, to overcome this, deuteration or single crystal studies are performed however in this study neither of these options was available to us. Hydrogen containing samples have been investigated using neutron powder diffraction in a wide range of areas from materials science to chemical reactivity and have been subject to a number of reviews (Weller *et al.*, 2009, Wilson *et al.*, 2014, Hansen & Kohlmann, 2014). One of the over-riding requirements is that high-flux instruments were required for the data collections.(Murshed & Kuhs, 2009, Murshed *et al.*, 2010) High-pressure neutron diffraction on hydrogenated materials has been conducted before on methane/CO2 gas hydrates (Staykova *et al.*, 2003) and brucite (Horita *et al.*, 2010) but the added sample environment can add further complications e.g. even higher backgrounds. One of the major developments at PEARL in recent years is the use of a neutron transparent ceramic, Zirconia Toughened Alumina (ZTA), and an alternative anvil material to the previously-used WC. (Bull *et al.*, 2016) At higher TOF (and longer d-spacing) the neutron transparency of the anvils allows a doubling of the signal compared to WC anvils with significantly reduced contamination in the diffraction pattern from the anvil material itself (Bull *et al.*, 2016). By using these anvils, we have

11

been able to collect data of sufficient quality on this weakly scattering solid for Rietveld refinement of the structure (Figure 2); the patterns shown in Figure 2 were collected for 4 hours. The data collection time of 8 hrs to obtain a pattern for Rietveld refinement typically compares with 4 hrs for a fully deuterated molecular organic solid. This is not ideal with limited allocations of beamtime however the advantages of being able to use a hydrogenated material without having to deuterate are significant. In particular, in cases where materials have altered properties in either their hydrogenated or deuterated form (highlighted below) or when the synthesis of deuterated materials is problematic such as is the case for glycolide.

The role of deuterium substitution may not have been systematically investigated, there are a number of studies that have identified changes in the phase behaviour of solids when this has occurred. This is a particularly important question if both neutron and X-ray techniques are being used to investigate the solid-state behaviour of materials. Two examples of the effects of deuteration on small molecules are observed with pyridine (Crawford *et al.*, 2009) and in acridine (Kupka *et al.*, 2012). The deuteration effect in pyridine was observed during a screen for new polymorphs which had been instigated by crystal structure predictions that showed a number of potential polymorphs equal in energy to the known Z'=4 structure but with Z'=1. All outcomes from the use of pyridine-h_5 in the crystallisations were the known form. Only when pyridine-d_5 was used did the authors isolate a new polymorph either from the pure compound or from a solution of pyridine-d_5 in pentane. The authors rationalised that the saturation solubility of pyridine-d_5 in pentane permitted the crystallisation below the phase transition hence the identification of the thermodynamically stable form at low temperature. At the same time, the high-resolution low-temperature neutron diffraction as well as high-pressure neutron diffraction measurements were being conducted, the latter being the only method by which both the –d_5 and –h_5 forms could crystallise in the Z'=1 structure.

The effect of deuteration on acridine was observed on crystallisation from acetone. Kupka *et al.* observed that either form-II (acridine-h_9) or form-III (acridine-d_9) could be crystallised from acetone as the pure polymorphs. In form-II all the molecules are associated via a dimer with CH…N interactions whilst form-III is a Z'=2 structure where molecules are linked through dimer interactions as well as a single C-D...N interaction. The authors investigated the intermolecular potentials for C-D…N and suggested that the substitution favoured the formation of additional C-D…N interactions. For a recent review of the effects of deuteration on organic systems as well as the effects of deuterated solvents on crystallisation, readers are directed to a review by Merz and Kupka (Merz & Kupka, 2015).

4. Concluding remarks

We have shown in this paper that we have been able to investigate the changes that occur in glycolide-h_4 to 6 GPa in the Paris-Edinburgh Press. The reconstructive nature of the phase transition

at 0.15 GPa necessitated the use of powder diffraction for sample analysis. The advantage of larger sample size afforded by the Paris Edinburgh and non-invasive nature of neutron radiation (over synchrotron source) made neutron powder diffraction the method of choice for our analysis. The use of hydrogenated material is a problem, however, the experiment has been enabled by the use of Zirconia Toughened Alumina anvils that possess neutron transparency compared with traditional tungsten carbide anvils. In this study we have observed that the phase transition to a previously identified high-pressure form (form-II) but at lower pressures than observed previously. This has been attributed to the use of the powdered form of glycolide in this experiment compared with previous work allowing for a rapid transition between the two phases. We have verified the existence and recovery of form-II under ambient conditions but due to time constraints were unable to assess its longevity at ambient pressure.

Supporting information
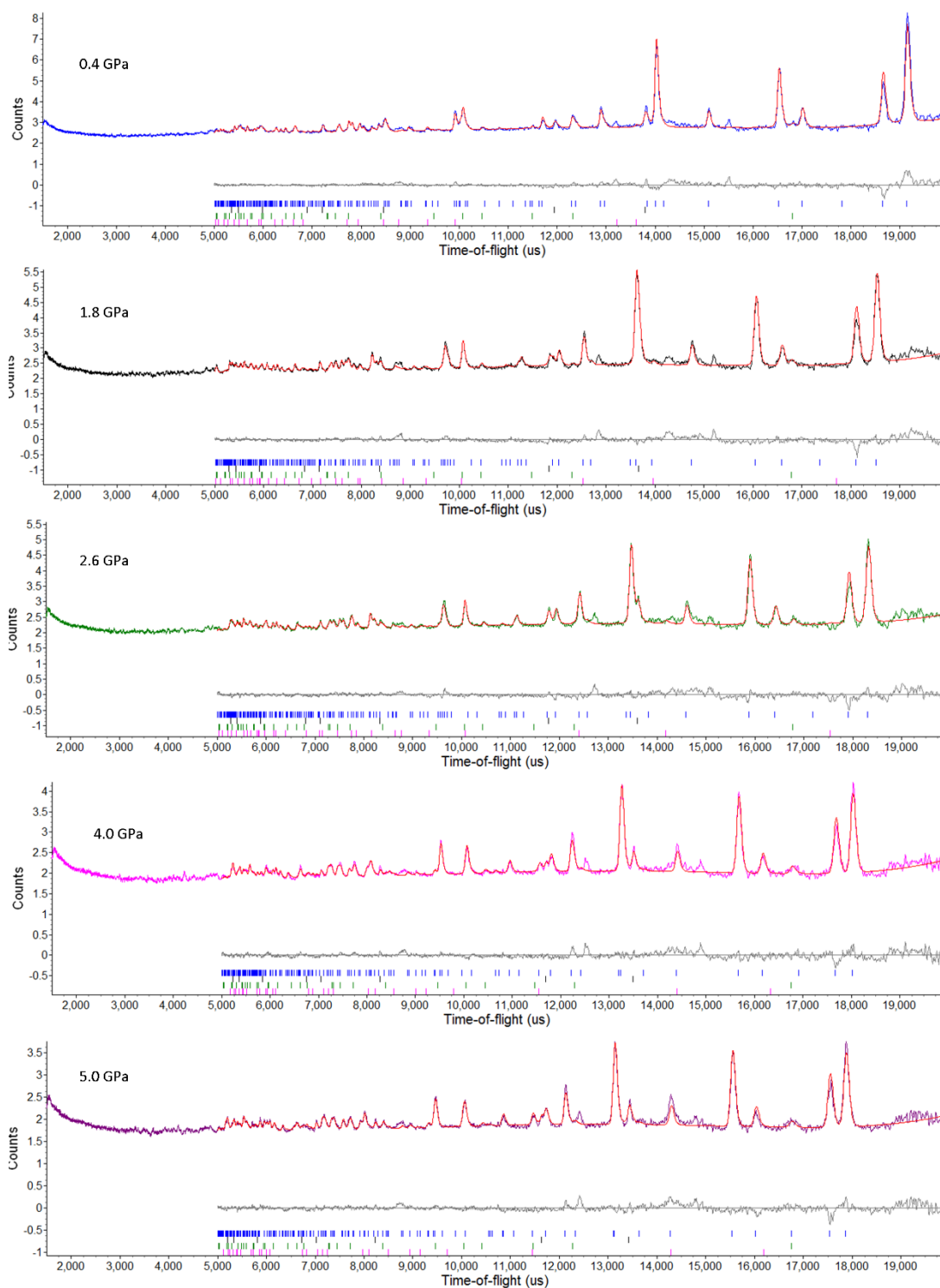
Figure S1   Rietveld refinements of glycolide-h$_4$ form-II at various pressures. All diffraction patterns show a good fit to the data. The crystal structure parameters can be found in Table S1.

Table S1   Refined unit cell parameters of glycolide on compression.

Pawley / Rietveld	Load (tonnes)	Form	Pressure (GPa)	Space Group	a-axis (Å)	b-axis (Å)	c-axis (Å)	β (°)	Unit Cell Volume (Å³)	Molecular Volume (Å³)	R_wp
Pawley	6	I	0.000(19)	$P2_1/n$	6.7037(7)	14.9640(17)	9.619(3)	98.884(15)	953.3(3)	119.1625	1.288
Pawley	9	I	0.031(14)	$P2_1/n$	6.689(3)	14.942(9)	9.610(5)	98.77(6)	949.3(9)	118.6625	1.157
Pawley	9	II	0.031(14)	$Pbca$	5.2240(8)	7.4321(11)	11.780(2)	90	457.35(13)	114.3375	1.157
Pawley	10	II	0.152(12)	$Pbca$	5.1906(4)	7.4150(5)	11.7692(15)	90	452.98(7)	113.245	1.887
Rietveld	12	II	0.406(9)	$Pbca$	5.1174(4)	7.3666(4)	11.7174(10)	90	441.71(6)	110.43	1.737
Pawley	14	II	0.64(2)	$Pbca$	5.0604(6)	7.3184(6)	11.6661(19)	90	432.05(9)	108.0125	2.04
Pawley	16	II	0.891(15)	$Pbca$	5.0252(5)	7.2861(7)	11.6373(19)	90	426.09(9)	106.5225	1.932
Pawley	18	II	1.07(3)	$Pbca$	5.0053(6)	7.2666(8)	11.6161(19)	90	422.49(10)	105.6225	2.077
Pawley	20	II	1.18(2)	$Pbca$	4.9859(5)	7.2512(7)	11.5914(18)	90	419.07(9)	104.7675	1.916
Pawley	23	II	1.43(3)	$Pbca$	4.9552(6)	7.2155(7)	11.560(2)	90	413.33(10)	103.3325	2.21
Rietveld	26	II	1.774(12)	$Pbca$	4.9209(4)	7.1818(5)	11.5243(10)	90	407.28(5)	101.805	1.606
Pawley	29	II	2.02(2)	$Pbca$	4.8989(7)	7.1545(8)	11.494(2)	90	402.86(11)	100.715	2.234
Pawley	32	II	2.35(2)	$Pbca$	4.8772(7)	7.1270(8)	11.468(3)	90	398.64(12)	99.66	2.279
Rietveld	35	II	2.574(14)	$Pbca$	4.8571(4)	7.1033(5)	11.4462(10)	90	394.91(5)	98.7375	1.620
Pawley	38	II	2.85(2)	$Pbca$	4.8401(7)	7.0825(8)	11.426(2)	90	391.69(11)	97.9225	2.139
Pawley	41	II	3.10(3)	$Pbca$	4.8253(8)	7.0650(10)	11.409(3)	90	388.95(13)	97.2375	2.539

Pawley	44	II	3.37(2)	*Pbca*	4.8107(8)	7.0402(10)	11.381(3)	90	385.44(13)	96.36	2.472
Pawley	47	II	3.68(3)	*Pbca*	4.7924(8)	7.0212(10)	11.356(3)	90	382.13(13)	95.5325	2.421
Rietveld	50	II	4.015(19)	*Pbca*	4.7757(4)	6.9930(5)	11.3384(10)	90	378.66(5)	94.665	1.660
Pawley	53	II	4.28(2)	*Pbca*	4.7615(8)	6.9771(11)	11.322(3)	90	376.14(13)	94.035	2.197
Pawley	56	II	4.65(2)	*Pbca*	4.7453(7)	6.9536(10)	11.303(2)	90	372.96(11)	93.24	1.868
Rietveld	59	II	5.01(3)	*Pbca*	4.7321(4)	6.9298(5)	11.2798(11)	90	369.89(6)	92.4675	1.795
Pawley	62	II	5.39(3)	*Pbca*	4.7196(8)	6.9133(13)	11.262(3)	90	367.45(14)	91.8625	2.384
Pawley	66	II	5.90(3)	*Pbca*	4.7009(9)	6.8872(14)	11.236(3)	90	363.78(15)	90.945	2.606

Table S2   PIXEL Energies and the partitioning into Coulombic, Polarisation, Dispersion and Repulsion terms (kJmol^{-1}) for Form II on increasing pressure.

Pressure	Distance	Coulombic Energy Component	Polarisation Energy Component	Dispersion Energy Component	Repulsion Energy Component	
Interaction 1: 0.5+x,1.5-y,1-z						
0.409	4.46	-21.5	-8.6	-21.4	29.2	-22.3
1.774	4.486	-21.4	-9	-21	28.5	-22.9
2.588	4.328	-26.7	-8.3	-21.6	35.1	-21.4
4.02	4.284	-27.8	-9.1	-23.1	39.9	-20.1
5.02	4.244	-30.2	-10.7	-25.2	47.3	-18.8
Interaction 2: 0.5+x,0.5-y,1-z						
0.409	4.51	-19.5	-5.5	-16.7	20.3	-21.4
1.774	4.224	-29.4	-9.7	-25.1	46.5	-17.7
2.588	4.277	-28.6	-12	-26.6	48.1	-19
4.02	4.184	-37	-16.3	-30.6	69.2	-14.7
5.02	4.148	-37.5	-15.8	-30.9	69.7	-14.4
Interaction 3: 1+x,y,z						
0.409	5.118	-10.3	-2.3	-9.3	5.4	-16.6
1.774	4.921	-13.7	-3.9	-13.2	14	-16.8
2.588	4.857	-15.6	-5	-15	19.3	-16.3
4.02	4.776	-19.8	-6	-17.2	27.5	-15.5
5.02	4.732	-21.7	-7.3	-18.7	33.8	-13.9
Interaction 4: 1-x,0.5+y,0.5-z						
0.409	6.923	-10.6	-2.4	-4.3	6.7	-10.5
1.774	6.715	-12.3	-3	-5.1	9.6	-10.7
2.588	6.754	-14.4	-3.7	-5.5	13	-10.6
4.02	6.686	-15.8	-4.4	-5.9	15.3	-10.8

5.02	6.65	-17.7	-5.3	-6.4	19.3	-10
Interaction 5: 1-x,0.5+y,1.5-z						
0.409	6.917	-7.6	-1.6	-3.9	3.8	-9.2
1.774	6.865	-11.3	-3	-5.2	10.1	-9.4
2.588	6.717	-11.9	-3	-5.3	10	-10.3
4.02	6.636	-13.9	-3.8	-6.1	14.1	-9.7
5.02	6.589	-16	-4.7	-6.4	17.2	-9.8
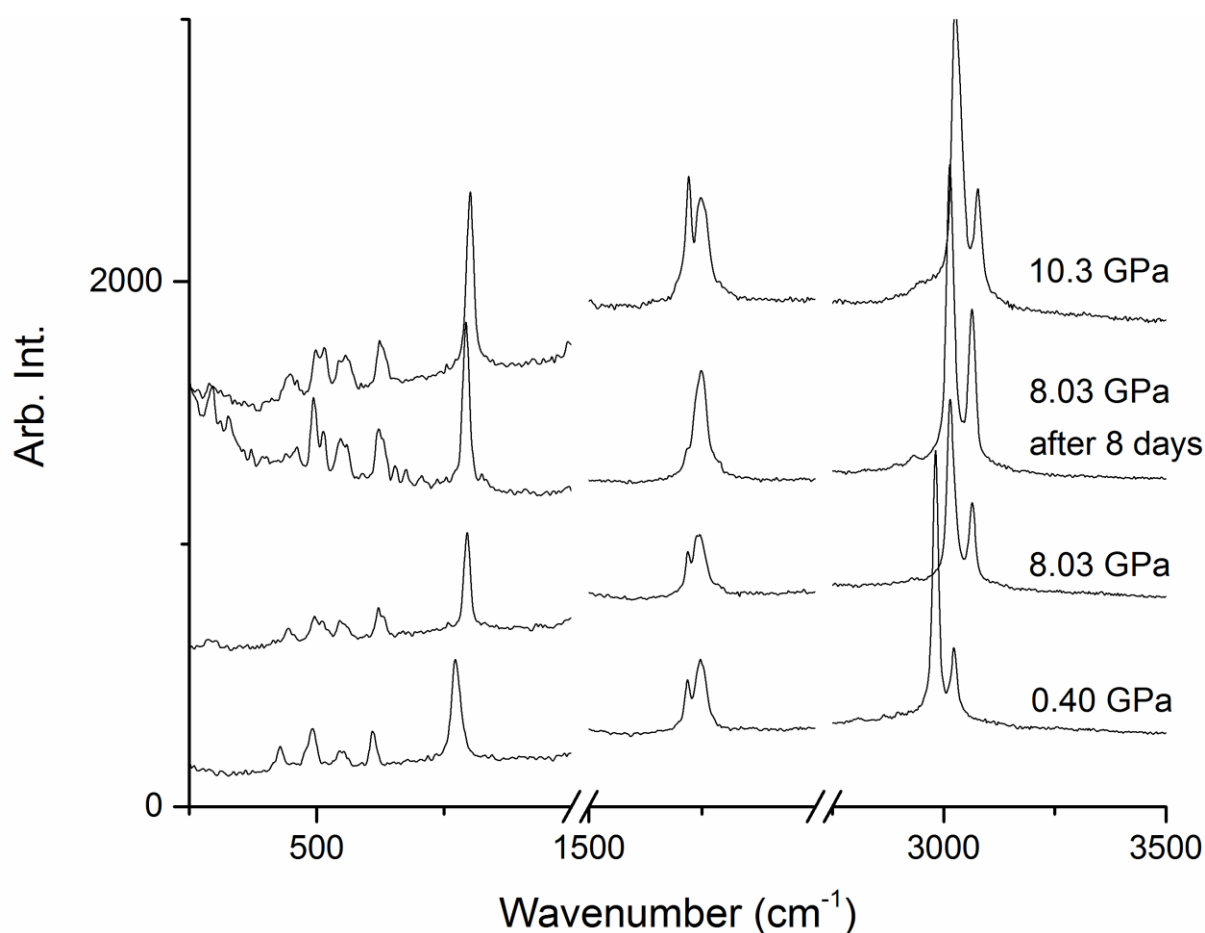
Figure S2 Raman spectra of glycolide at 0.40 GPa, 8.03 GPa on the same day and after 8 days at 8.03 GPa (Pressure of cell was 8.5 GPa on day 8) and subsequent compression to 10.3 GPa. There is little difference in the spectra showing that no reaction has occurred during the day. The breaks in the x-axis correspond with primary and secondary diamond vibrations.

5. References

Allen, F. H., Baalham, C. A., Lommerse, J. P. M. & Raithby, P. R. (1998). *Acta Crystallographica Section B-Structural Science* **54**, 320-329.

Angel Ross, J., Alvaro, M. & Gonzalez-Platas, J. (2014). EosFit7c and a Fortran module (library) for equation of state calculations, Vol. 229, Zeitschrift für Kristallographie - Crystalline Materials, p. 405.

Aoki, K., Kakudate, Y., Yoshida, M., Usuba, S. & Fujiwara, S. (1989). *J. Chem. Phys.* **91**, 778-782.

Bergantin, S., Moret, M., Buth, G. & Fabbiani, F. P. A. (2014). *Journal of Physical Chemistry C* **118**, 13476-13483.

Bini, R., Ceppatelli, M., Citroni, M. & Schettino, V. (2012). *Chem. Phys.* **398**, 262-268.

Bond, A. D. (2014). *Journal of Applied Crystallography* **47**, 1777-1780.

Bull, C. L., Funnell, N. P., Tucker, M. G., Hull, S., Francis, D. J. & Marshall, W. G. (2016). *High Pressure Research* **36**, 493-511.

Ceppatelli, M., Frediani, M. & Bini, R. (2011). *Journal of Physical Chemistry B* **115**, 2173-2184.

Ceppatelli, M., Santoro, M., Bini, R. & Schettino, V. (2000). *J. Chem. Phys.* **113**, 5991-6000.

Chelazzi, D., Ceppatelli, M., Santoro, M., Bini, R. & Schettino, V. (2005). *Journal of Physical Chemistry B* **109**, 21658-21663.

Ciabini, L., Santoro, M., Bini, R. & Schettino, V. (2002). *J. Chem. Phys.* **116**, 2928-2935.

Ciabini, L., Santoro, M., Gorelli, F. A., Bini, R., Schettino, V. & Raugei, S. (2007). *Nature Materials* **6**, 39-43.

Coelho, A. (2012). *TOPAS – Academic: General Profile and Structure Analysis Software for Powder Diffraction Data.* Version Version 5.

Crawford, S., Kirchner, M. T., Blaser, D., Boese, R., David, W. I. F., Dawson, A., Gehrke, A., Ibberson, R. M., Marshall, W. G., Parsons, S. & Yamamuro, O. (2009). *Angew. Chem.-Int. Edit.* **48**, 755-757.

Dechy-Cabaret, O., Martin-Vaca, B. & Bourissou, D. (2004). *Chemical Reviews* **104**, 6147-6176.

Fabbiani, F. P. A., Allan, D. R., David, W. I. F., Davidson, A. J., Lennie, A. R., Parsons, S., Pulham, C. R. & Warren, J. E. (2007). *Cryst. Growth Des.* **7**, 1115-1124.

Frisch, M. J., Trucks, G. W., Schlegel, H. B., Scuseria, G. E., Robb, M. A., Cheeseman, J. R., Scalmani, G., Barone, V., Mennucci, B., Petersson, G. A., Nakatsuji, H., Caricato, M., Li, X., Hratchian, H. P., Izmaylov, A. F., Bloino, J., Zheng, G., Sonnenberg, J. L., Hada, M., Ehara, M., Toyota, K., Fukuda, R., Hasegawa, J., Ishida, M., Nakajima, T., Honda, Y., Kitao, O., Nakai, H., Vreven, T., Montgomery, J. A., Peralta, J. E., Ogliaro, F., Bearpark, M., Heyd, J. J., Brothers, E., Kudin, K. N., Staroverov, V. N., Kobayashi, R., Normand, J., Raghavachari, K., Rendell, A., Burant, J. C., Iyengar, S. S., Tomasi, J., Cossi, M., Rega, N., Millam, J. M., Klene, M., Knox, J. E., Cross, J. B., Bakken, V., Adamo, C., Jaramillo, J., Gomperts, R., Stratmann, R. E., Yazyev, O., Austin, A. J., Cammi, R., Pomelli, C., Ochterski, J. W., Martin, R. L., Morokuma, K., Zakrzewski, V. G., Voth, G. A., Salvador, P., Dannenberg, J. J., Dapprich, S., Daniels, A. D., Farkas, Foresman, J. B., Ortiz, J. V., Cioslowski, J. & Fox, D. J. (2009). Gaussian 09, Revision B.01, Wallingford CT.

Funnell, N. P., Marshall, W. G. & Parsons, S. (2011). *CrystEngComm* **13**, 5841-5848.

Gavezzotti, A. (2011). *New Journal of Chemistry* **35**, 1360-1368.

Gould, R. O., Taylor, P. & Thorpe, M. (1995). *Pucker.* Version 7.7.95.

Hansen, T. C. & Kohlmann, H. (2014). *Zeitschrift für anorganische und allgemeine Chemie* **640**, 3044-3063.

Hobday, C. L., Marshall, R. J., Murphie, C. F., Sotelo, J., Richards, T., Allan, D. R., Duren, T., Coudert, F. X., Forgan, R. S., Morrison, C. A., Moggach, S. A. & Bennett, T. D. (2016). *Angew. Chem.-Int. Edit.* **55**, 2401-2405.

Horita, J., dos Santos, A. M., Tulk, C. A., Chakoumakos, B. C. & Polyakov, V. B. (2010). *Physics and Chemistry of Minerals* **37**, 741-749.

Hutchison, I. B., Delori, A., Wang, X., Kamenev, K. V., Urquhart, A. J. & Oswald, I. D. H. (2015). *Crystengcomm* **17**, 1778-1782.

Jin, H. J., Plonka, A. M., Parise, J. B. & Goroff, N. S. (2013). *Crystengcomm* **15**, 3106-3110.

Johnston, B. F., Marshall, W. G., Parsons, S., Urquhart, A. J. & Oswald, I. D. H. (2014). *The Journal of Physical Chemistry B* **118**, 4044-4051.

Klotz, S., Chervin, J. C., Munsch, P. & Le Marchand, G. (2009). *J. Phys. D-Appl. Phys.* **42**, 7.

Kojima, Y., Matsuoka, T., Sato, N. & Takahashi, H. (1995). *Journal of Polymer Science Part a-Polymer Chemistry* **33**, 2935-2940.

Kupka, A., Vasylyeva, V., Hofmann, D. W. M., Yusenko, K. V. & Merz, K. (2012). *Cryst. Growth Des.* **12**, 5966-5971.

Macrae, C. F., Bruno, I. J., Chisholm, J. A., Edgington, P. R., McCabe, P., Pidcock, E., Rodriguez-Monge, L., Taylor, R., van de Streek, J. & Wood, P. A. (2008). *Journal of Applied Crystallography* **41**, 466-470.

Mao, H. K., Wu, Y., Shu, J. F., Hu, J. Z., Hemley, R. J. & Cox, D. E. (1990). *Solid State Communications* **74**, 1027-1029.

Marshall, W. G. & Francis, D. J. (2002). *Journal of Applied Crystallography* **35**, 122-125.

Marshall, W. G., Urquhart, A. J. & Oswald, I. D. H. (2015). *Journal of Physical Chemistry B* **119**, 12147-12154.

Merz, K. & Kupka, A. (2015). *Cryst. Growth Des.* **15**, 1553-1558.

Moggach, S. A., Parsons, S. & Wood, P. A. (2008). *Crystallography Reviews* **14**, 143-183.

Murli, C., Mishra, A. K., Thomas, S. & Sharma, S. M. (2012). *The Journal of Physical Chemistry B* **116**, 4671-4676.

Murli, C. & Song, Y. (2010). *Journal of Physical Chemistry B* **114**, 9744-9750.

Murshed, M. M. & Kuhs, W. F. (2009). *The Journal of Physical Chemistry B* **113**, 5172-5180.

Murshed, M. M., Schmidt, B. C. & Kuhs, W. F. (2010). *J. Phys. Chem. A* **114**, 247-255.

Oehzelt, M., Aichholzer, A., Resel, R., Heimel, G., Venuti, E. & Della Valle, R. G. (2006). *Physical Review B* **74**, 104103.

Olejniczak, A., Krukle-Berzina, K. & Katrusiak, A. (2016). *Cryst. Growth Des.* **16**, 3756-3762.

Oswald, I. D. H., Hamilton, A., Hall, C., Marshall, W. G., Prior, T. J. & Pulham, C. R. (2008). *J. Am. Chem. Soc.* **130**, 17795-17800.

Oswald, I. D. H. & Pulham, C. R. (2008). *Crystengcomm* **10**, 1114-1116.

Oswald, I. D. H. & Urquhart, A. J. (2011). *Crystengcomm* **13**, 4503-4507.

Santoro, M., Ciabini, L., Bini, R. & Schettino, V. (2003). *Journal of Raman Spectroscopy* **34**, 557-566.

Schulte, O. & Holzapfel, W. B. (1995). *Physical Review B* **52**, 12636-12639.

Sun, J. M., Dong, X., Wang, Y. J., Li, K., Zheng, H. Y., Wang, L. J., Cody, G. D., Tulk, C. A., Molaison, J. J., Lin, X. H., Meng, Y. F., Jin, C. Q. & Mao, H. K. (2017). *Angew. Chem.-Int. Edit.* **56**, 6553-6557.

Vohra, Y. K. & Ruoff, A. L. (1990). *Physical Review B* **42**, 8651-8654.

Weller, M. T., Henry, P. F., Ting, V. P. & Wilson, C. C. (2009). *Chemical Communications*, 2973-2989.

Wilhelm, C., Boyd, S. A., Chawda, S., Fowler, F. W., Goroff, N. S., Halada, G. P., Grey, C. P., Lauher, J. W., Luo, L., Martin, C. D., Parise, J. B., Tarabrella, C. & Webb, J. A. (2008). *J. Am. Chem. Soc.* **130**, 4415-4420.

Wilson, C. C., Henry, P. F., Schmidtmann, M., Ting, V. P., Williams, E. & Weller, M. T. (2014). *Crystallography Reviews* **20**, 162-206.

Wood, P. A., Francis, D., Marshall, W. G., Moggach, S. A., Parsons, S., Pidcock, E. & Rohl, A. L. (2008). *Crystengcomm* **10**, 1154-1166.

Zakharov, B. A. & Boldyreva, E. V. (2014). *Journal of Molecular Structure* **1078**, 151-157.

Zakharov, B. A., Goryainov, S. V. & Boldyreva, E. V. (2016). *Crystengcomm* **18**, 5423-5428.

Zakharov, B. A., Seryotkin, Y. V., Tumanov, N. A., Paliwoda, D., Hanfland, M., Kurnosov, A. V. & Boldyreva, E. V. (2016). *RSC Advances* **6**, 92629-92637.